JCTC Journal of Chemical Theory and Computation

Article

pubs.acs.org/JCTC

Toward Reliable Prediction of Hyperfine Coupling Constants Using *Ab Initio* Density Matrix Renormalization Group Method: Diatomic $^2\Sigma$ and Vinyl Radicals as Test Cases

Tran Nguyen Lan,*[,†] Yuki Kurashige,[†,‡] and Takeshi Yanai[†,‡]

[†]The Graduate University for Advanced Studies, Myodaiji, Okazaki, Aichi 444-8585, Japan

[‡]Department of Theoretical and Computational Molecular Science, Institute for Molecular Science, Okazaki, Aichi 444-8585, Japan

ABSTRACT: The density matrix renormalization group (DMRG) method is used in conjunction with the complete active space (CAS) procedure, the CAS configuration interaction (CASCI), and the CAS self-consistent field (CASSCF) to evaluate hyperfine coupling constants (HFCCs) for a series of diatomic $^2\Sigma$ radicals (BO, CO^+, CN, and AlO) and vinyl (C_2H_3) radical. The electron correlation effects on the computed HFCC values were systematically investigated using various levels of active space, which were increasingly extended from single valence space to large-size model space entailing double valence and at least single polarization shells. In addition, the core correlation was treated by including the core orbitals in active space. Reasonably accurate results were obtained by the DMRG-CASSCF method involving orbital optimization, while DMRG-CASCI calculations with Hartree−Fock orbitals provided poor agreement of the HFCCs with the experimental values. To achieve further insights into the accuracy of HFCC calculations, the orbital contributions to the total spin density were analyzed at a given nucleus, which is directly related to the FC term and is numerically sensitive to the level of correlation treatment and basis sets. The convergence of calculated HFCCs with an increasing number of renormalized states was also assessed. This work serves as the first study on the performance of the *ab initio* DMRG method for HFCC prediction.

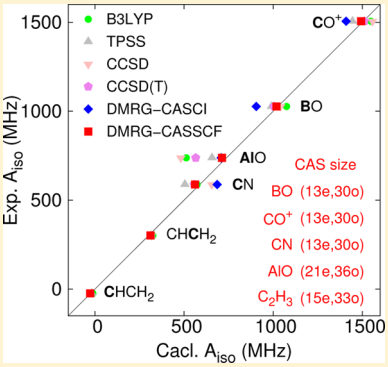

1. INTRODUCTION

The hyperfine coupling constant (HFCC) is an observation of the interaction between electron spin **s** and nuclear spin **I** that plays an important role in understanding molecular electron paramagnetic resonance (EPR) spectra.[1] There are both isotropic and anisotropic contributions to HFCCs. For light element molecules, the spin−orbit coupling (SOC) is small and can be neglected, so that the HFCCs are dominated by the Fermi contact (FC) term[2] and the spin-dipole (SD) interaction term.[3] While the SD term is known to be numerically less sensitive and thus can be relatively easily calculated, the high-accuracy prediction of the FC term is still a challenging task for computational quantum chemistry. Difficulties arise because the FC term is evaluated from a direct numerical measure of the spin density at the position of the nucleus, which is quite sensitive to the quality of the electronic structure calculation. Therefore, high-level treatment of the wave function involving electron correlation and the basis sets is often required to achieve sufficient accuracy in HFCC calculations. The effects of the basis set on the FC term are caused in close proximity to the nuclear centers, so that the tight Gaussian-type functions are also used. The solvent and vibrational effects are also important in extreme cases.[4] However, it is quite difficult and expensive to account for these effects in *ab initio* quantum chemistry calculations. The nonvibrating gas-phase condition has been widely adopted for HFCC calculations and is also assumed in this study. In addition, we only focus on the nonrelativistic limit in the present work.

The restricted open-shell Hartree−Fock (ROHF) method cannot describe the core level spin-polarization;[5] therefore, it is incapable of describing the FC term. In contrast, the spin-polarization is explicitly included in the unrestricted Hartree−Fock (UHF) method. However, the UHF method typically overestimates the FC term to a large extent due to the mean-field treatment of many-electron interactions. Spin contamination in the UHF wave function is considered to be another source of errors. To remedy the spin-contamination effect, Nakatsuji et al.[6] developed a modified UHF, the projected UHF (PUHF). Although this method certainly provides an improvement of the UHF results, it does not give uniform agreement with experimental results better than approximately 60%, as shown by Chipman.[7] These earlier studies showed that electron correlation effects are largely responsible for accuracy of HFCC calculations.

The coupled cluster (CC) approach has been widely applied to HFCC calculations. Bartlett and co-workers developed several approaches based on the CC framework to evaluate the HFCCs, including finite-field CC[8] or analytical derivative CC.[9] Later, they used the two-parameter complete basis set (CBS2) extrapolation scheme in the CC calculations of HFCCs to rectify the error from basis set truncation.[10] Their benchmarks revealed that the calculated FC values are strongly dependent on the choice of basis set and treatment with and without the

Received: November 11, 2013
Published: January 28, 2014

perturbative triples, as well as the type of reference wave functions (UHF or ROHF). In addition, the core correlation was determined as necessary for FC calculations of non-hydrogen atoms. Recently, Puzzarini and Barone[11−15] provided a series of assessments on the performance of CC methods in conjunction with the CBS2 extrapolation for organic free radicals. The results showed remarkable agreement with the experimental data.

Momose et al.[16,17] employed the symmetry adapted cluster−configuration interaction (SAC−CI) method to evaluate the HFCCs of several organic radicals. The results obtained using the Dunning double-zeta basis set (DZ) were in fair agreement with the experimental results. However, such agreement was shown to be fortuitous and was the result of error cancellations because the DZ basis set is not sufficiently large and flexible to provide accurate HFCCs.[18]

Chipman systematically assessed the influence of excitation levels of the configuration interaction (CI) method for treatment of HFCCs for the CH radical,[7] which revealed a nonmonotonic variation of the FC value for the C center with increasing CI excitation levels. CI with single and double excitations (CISD) gives an error of more than 30%, while good agreement with experimental value can be obtained with CI including only single excitation (CIS). An almost converged value was finally realized when all triple excitations (CISDT) were taken into account. Chipman thus asserted that the doubles corrections to the HFCCs were important due to the pair correlations, but this led to poor agreement. However, the contributions to the HFCCs from the triples often cancel out those from the doubles. Therefore, the simplest spin polarization model based on the CIS scheme may be sufficiently accurate for the prediction of HFCCs. However, the CIS is the subspace of the CISD, so that the success of such an inexpensive method seems to be due to some sort of error cancellation, as shown later by Engels.[19] The increasing excitation levels of CI treatment offer two distinct contributions to the FC term: direct and indirect effects. First, as the CI level is promoted form CIS to CISD, the direct effect arises as nonzero coefficients of the double excitations. Second, through the interactions within the CI Hamiltonian matrix, the inclusion of double excitations makes certain change in the resultant CI coefficients of the reference and singly excited determinants relative to those obtained by the CIS treatment. This effect is called the indirect effect of the double excitation on the FC term. Engels found that these two effects have opposite signs, and the absolute amplitude of the indirect effect is much higher than that of the direct effect, which leads to a significant change of the net spin density when the method level goes from CIS to CISD. Finally, the direct and indirect effects with inclusion of the higher excitations (triples or higher) tend to cancel each other to a great extent, so that a converged value can then be obtained. This is also the reason for the fortuitous agreement of the CIS results with the experimental data reported by Chipman. Another important conclusion from Engels' work is that the indirect effect of triples and quadruples is much more significant than their direct contribution. Therefore, Engels' finding provided some valuable insight into why the CC singles and doubles (CCSD) as well as the quadratic configuration interaction singles and doubles (QCISD) approaches, which encompass higher excitation levels arising from the disconnected clusters, give accurate HFCCs in most cases.

Although higher excitation configurations from the Hartree−Fock (HF) reference are crucial to achieve *realistic* accuracy in the CI calculations of HFCCs, they are sometimes too expensive to compute. As an alternative CI treatment, the multireference configuration interaction (MR-CI) is employed to efficiently include the high-level correlation in some sense. In earlier studies, the performance of MR-CI to obtain HFCCs was shown to be dependent on the choice of orbital transformations, such as HF molecular orbitals, natural orbitals, and spin natural orbitals.[20,21] In addition to the orbital shape, the procedure to expand the MR-CI wave function has a strong effect on the FC term. It is often impossible to include all singles and doubles from the set of multiple reference configurations; therefore, the so-called "selection" procedure is combined with MR-CI calculations to effectively truncate the CI space to a tractable size.[20,22,23] However, Bauschlicher[24] and Engels[25] concluded that the conventional selection procedures fail to recover important configurations for the FC term. To rectify this inadequacy, Engels[25,26] developed a modified selection method. Perturbation techniques, the so-called B_K and A_K procedures,[27−30] were thus employed to recover the indirect effects arising from configurations neglected in the traditional MR-CI truncation. This approach was applied to several small molecules and generally provided HFCCs that agreed well with the experimental results.[25,26,31−33]

Kristiansen and Veseth[34,35] first used the many-body perturbation theory (MBPT) up to the third-order to calculate the HFCCs for hydrides and generally found good agreement between the computed and experimental results. Gauld et al.[36] performed an assessment study of the unrestricted second-order Møller−Plesset (UMP2) theory to calculate HFCCs of radical systems with the 6−311+G(2df,p) basis set. Although the use of the UMP2 method results in marked improvements over the UHF method, the errors relative to the experimental values remain large. Recently, the HFCCs of nitrogen and phosphorus atoms were evaluated using the MP2 and MP4 approaches by Kaupp et al.[37] The accuracy of MP2 was shown to be clearly unacceptable, while MP4 gave greatly improved agreement with the experimental data. Kossmann and Neese[38] assessed the performance of orbital-optimization MP2 (OO-MP2) methods (with and without spin-component-scaling) for the computation of HFCCs. Surprisingly, the results of OO-MP2 are comparable with those of CCSD and QCISD methods for small radicals. The low computational cost of the OO-MP2 methods make them promising for application to large organic molecules.

An alternative electronic structure method to calculate HFCCs is the density functional theory (DFT).[39−51] The main advantage of DFT is the low computational and memory requirements. Among the functionals tested, the hybrid functionals such as B3LYP[52,53] and PBE0[54,55] are known to perform best in many cases. In a recent assessment of DFT performance, Kossmann et al.[47] have shown that the meta-GGA functional TPSS[56] (and its hybrid version TPSSh[56]) and the double hybrid functional B2PLYP[57] provide the HFCCs in acceptable agreement with experimental results. While DFT provides HFCCs with accuracy comparable to that of the MR-CI or CCSD(T) levels of theory for light main group radicals, it has difficulty producing similar accuracy for isolated atoms, radicals containing electronegative elements, and transition metal complexes.[44] The successful accuracy of this method is sometimes attributed to fortuitous error cancellations.[58] In addition, it is recognized that the exchange-correlation functionals for appropriate prediction of HFCCs are largely

system-dependent in difficult cases, especially for transition metal complexes.[40,44,47]

Despite the recent progress, it is still important and challenging to provide highly reliable values of the HFCCs, even for small molecules, from quantum chemical calculations that are numerically convergent with respect to the level of the theoretical treatment. In this study, we attempt to use the density matrix renormalization group (DMRG) method[59−60] with large active space to include near convergent electron correlation in the HFCC calculations. The DMRG method was introduced in condensate-matter physics by White,[59,60] and later applied to *ab initio* quantum chemical calculations.[61−70] The DMRG method has been shown to be an exceedingly efficient approach to a near "exact" [or full CI (FCI)] solution. In this algorithm, the molecular orbitals (MOs) are assigned to 1D quantum lattice sites. The tractable correlation length in the 1D lattice is controlled by the number of renormalized basis states M, which affects the computational cost as $O(M^3k^3 + M^2k^4)$, where k refers to the number of MOs.

Although the DMRG method can be used in a brute-force way as a highly scalable substitute for the FCI, recent studies have shown that it can be more practically used in combination with the complete active space (CAS) model to describe the multireference (or active-space) correlation. This active-space DMRG approach has been combined with the orbital optimization procedure[68,71,72] and is able to go far beyond the limitation of the traditional complete active space self-consistent field (CASSCF) method. In practical applications, the DMRG method has been shown to be successful for the prediction of molecular properties in large-scale multireference states.[69,73−82] Most recently, Boguslawski et al. demonstrated that a reliable spin density can be calculated using the DMRG algorithm[83] and concluded that reliable reference spin densities can be obtained even if the total energies are not converged with respect to M. Besides the fixed M strategy, more reliable extrapolation scheme is perhaps possible using entanglement entropy optimization tools,[84−85] while in the present work fixed M calculations are performed and convergence rate is analyzed as a function of M.

This article reports the initial application of the DMRG algorithm in combination with complete active configuration interaction (CASCI) and CASSCF methods for computing the HFCCs, the FC and SD terms. The electron correlation effects on the computed HFCC values are systematically investigated using various levels of active space, which are increasingly extended from the single valence space to the large model space entailing double valence and at least single polarization shells. In addition, the core correlation is treated by including the core orbitals in active space. High-accuracy wave functions are obtained using the DMRG-CASCI and DMRG-CASSCF calculations with large-size active space. The exact diagonalization with such active space can be achieved only by the DMRG method. The dependence of the formulas for the FC and SD terms on the DMRG wave function arises through the spin density. The DMRG with enlargement of the active space delivers convergence of the spin density to a FCI-quality description. To achieve further insights into the accuracy of HFCC calculations, the orbital contributions to the total spin density are analyzed at a given nucleus, which is directly related to the FC term and is numerically sensitive to the level of correlation treatment and basis sets.

In this study, assessment of the DMRG method for HFCC calculations is first performed on small $^2\Sigma$ radicals: BO, CO^+, CN, and AlO. Although these test molecules are small in size, determination of their HFCCs is considered to be important from both experimental and computational perspectives. Moreover, it is of significant value to provide theoretical values with near exact accuracy that can serve as benchmark data. The HFCCs of BO and CO^+ have been well characterized by the conventional methods, namely DFT and CC, to an acceptable accuracy with respect to the experimental values. However, the determination of HFCCs for the CN and AlO molecules is a challenge for the computational approaches. The difficulties are that the unrestricted treatment for CN suffers from a large degree of spin contamination,[36] and the delicate balance between the ionic states of AlO must be handled carefully in the electronic structure calculations.[86−90] Finally, to explore the performance of present approach for HFCC prediction of multiatomic organic radicals, we evaluate the HFCCs of vinyl (C_2H_3) radical. We concomitantly address the following questions of technical interest: (i) Can HFCCs be accurately described by the active-space wave function? (ii) What type of orbitals should be included in active space for HFCC calculations? We attempt to address these issues using the active-space DMRG method.

The paper is organized as follows. In section 2, we briefly discuss the background of quantum chemical calculations for the hyperfine coupling tensors. The computational details are shown in section 3. The results are presented and discussed in section 4. Finally, a summary and concluding remarks are given in section 5.

2. THEORETICAL BACKGROUND

2.1. Hyperfine Coupling Tensor. The hyperfine coupling tensor $\mathbf{A}$ is parametrized by a phenomenological spin-Hamiltonian that describes the interaction between electron spin $\mathbf{s}$ and nuclear spin $\mathbf{I}$: $\hat{H}_{SI} = \mathbf{s}\cdot\mathbf{A}\cdot\mathbf{I}$. In the absence of SOC, this Hamiltonian contains two terms; the Fermi-contact Hamiltonian,[2]

$$\hat{H}_{FC} = \frac{8\pi}{3} g_e\beta \sum_K g_K\beta_K \sum_i \left[\delta(r_{iK})\mathbf{s}_i\mathbf{I}^{(K)}\right] \tag{1}$$

and the spin-dipole Hamiltonian,[3]

$$\hat{H}_{SD} = g_e\beta \sum_K g_K\beta_K \sum_i \left[\frac{\mathbf{s}_i\mathbf{I}^{(K)}}{r_{iK}^3} - 3\frac{(\mathbf{s}_i\mathbf{r}_{iK})(\mathbf{I}^{(K)}\mathbf{r}_{iK})}{\mathbf{r}_{iK}^5}\right] \tag{2}$$

where K and i run over the number of nuclei and electrons, respectively. The constant g_e is the g-value of a free electron (g_e = 2.002319), β is the Bohr magneton, g_K and β_K are the nuclear g-value and nuclear magneton of a given nucleus K, respectively. $\mathbf{r}_{iK}(= (r_{iK,x}, r_{iK,y}, r_{iK,z}))$ is the distance vector between the i-th electron and K-th nucleus. The symbol $\delta(...)$ refers to the Dirac delta function. The $\mathbf{A}$ tensor of nucleus K is obtained by taking the second derivative of the spin-Hamiltonian with respect to electron and nuclear spins:

$$\mathbf{A}^{(K)} = \frac{\partial^2\hat{H}_{SI}}{\partial\mathbf{s}\,\partial\mathbf{I}} \tag{3}$$

This can be expressed as the decomposed form:

$$\mathbf{A}^{(K)} = \mathbf{A}^{(K;c)} + \mathbf{A}^{(K;d)} \tag{4}$$

with the FC tensor $\mathbf{A}^{(K;c)}$,

dx.doi.org/10.1021/ct400978j | J. Chem. Theory Comput. 2014, 10, 1953−1967

Table 1. Active Orbitals

molecule	active space	active orbitals	
BO, CO^+, and CN	CAS(9e,8o)	B, C, O, N: 2s2p	
	CAS(9e,16o)	B, C, O, N: 2s2p3s3p	
	CAS(9e,28o)	B, C, O, N: 2s2p3s3p4s3d	
	CAS(13e,30o)	B, C, O, N: 1s2s2p3s3p4s3d	
AlO	CAS(9e,8o)	Al: 3s3p O: 2s2p	
	CAS(9e,16o)	Al: 3s3p3d O: 2s2p3p	
	CAS(9e,21o)	Al: 3s3p3d	O: 2s2p3p,3d
	CAS(15e,28o)	Al: 2p3s3p3d4p	O: 2s2p3s3p3d
	CAS(21e,31o)	Al: 1s2s2p3s3p3d4p	O: 1s2s2p3s3p3d
	CAS(15e,33o)	Al: 2p3s3p3d4p4d	O: 2s2p3s3p3d
	CAS(21e,36o)	Al: 1s2s2s2p3s3p3d4p4d	O: 1s2s2p3s3p3d
C_2H_3	CAS(15e,33o)	C: 1s2s2p3s3p4s3d	H: 1s

$$A_{kl}^{(K;c)} = \delta_{kl}\frac{8\pi}{3}\frac{P_K}{2S}\sum_{\mu\nu}P_{\mu\nu}^{(\alpha-\beta)}\left\langle \chi_\mu \middle| \delta(r_{iK}) \middle| \chi_\nu \right\rangle \tag{5}$$

and the SD tensor $\mathbf{A}^{(K;d)}$,

$$A_{kl}^{(K;d)} = \frac{P_K}{2S}\sum_{\mu\nu}P_{\mu\nu}^{(\alpha-\beta)}\left\langle \chi_\mu \middle| r_{iK}^{-5}(r_{iK}^2\delta_{kl} - 3r_{iK,k}r_{iK,l}) \middle| \chi_\nu \right\rangle \tag{6}$$

where $k,l = x,y,z$; $P_K(= g_e\beta g_K\beta_K)$ is the nucleus-type constant; and S is the total spin. The one-particle integrals $\langle \chi_\mu|...|\chi_\nu \rangle$ in eqs 5 and 6 are represented in atomic orbital (AO) basis χ_μ and χ_ν. The FC integral is regarded as the overlap distribution at the nuclear point K. The implementation of the SD integral is more complicated than that of the FC integral. The SD integral was implemented using the Rys-quadrature algorithm.[91] The matrix $P_{\mu\nu}^{(\alpha-\beta)}$ is the difference between the α and β electron density matrices in the AO basis representation, which is referred to as the AO spin density matrix.

2.2. Spin Density Analysis. The spatially resolved spin density can be given by

$$\rho^{(\alpha-\beta)}(\mathbf{r}) = \sum_{\mu\nu}P_{\mu\nu}^{(\alpha-\beta)}\chi_\mu(\mathbf{r})\chi_\nu(\mathbf{r}) = \sum_{\mu\nu}\sum_{pq}^{\mathrm{MO}}D_{pq}^{(\alpha-\beta)}c_{p\mu}c_{q\nu}\chi_\mu(\mathbf{r})\chi_\nu(\mathbf{r}) \tag{7}$$

where the matrix $D_{pq}^{(\alpha-\beta)}$ is the spin density matrix represented in the given MO basis, thus referred to as the MO spin density matrix, and $c_{p\mu}$ are the MO coefficients. Diagonalization of the MO spin density matrix leads to the so-called spin natural orbitals (SNOs). Let $n_i^{(\alpha-\beta)}$ and U_{ip} be its eigenvalues and eigenvectors, respectively, so that we have $\Sigma_{pq}U_{ip}U_{jq}D_{pq}^{(\alpha-\beta)} = \delta_{ij}n_i^{(\alpha-\beta)}$ The MO coefficients of the SNOs, $\{\bar{c}_{i\mu}\}$, can be obtained from the unitary transformation of $\{c_{p\mu}\}$ as

$$\bar{c}_{i\mu} = \sum_{p}^{\mathrm{MO}}U_{ip}c_{p\mu} \tag{8}$$

This definition is analogous to that for the natural orbitals (NOs) obtained by diagonalization of the density matrix. The eigenvalue $n_i^{(\alpha-\beta)}$ is called the spin occupation number of the i-th SNO. The spatially resolved spin density $\rho^{(\alpha-\beta)}(\mathbf{r})$ (eq7) can be rewritten using the SNO basis as follows:

$$\rho^{(\alpha-\beta)}(\mathbf{r}) = \sum_{i}^{\mathrm{SNO}}\sum_{\mu\nu}n_i^{(\alpha-\beta)}\bar{c}_{i\mu}\bar{c}_{i\nu}\chi_\mu(\mathbf{r})\chi_\nu(\mathbf{r}) \tag{9}$$

Finally, the spatially resolved spin density $\rho^{(\alpha-\beta)}(\mathbf{r})$ can be written as the summation of individual SNO contributions:

$$\rho^{(\alpha-\beta)}(\mathbf{r}) = \sum_{i}^{\mathrm{SNO}}\rho_i^{(\alpha-\beta)}(\mathbf{r}) \tag{10}$$

where $\rho_i^{(\alpha-\beta)}(\mathbf{r})$ is the spatial distribution of the spin density associated with the i-th SNO, given by

$$\rho_i^{(\alpha-\beta)}(\mathbf{r}) = n_i^{(\alpha-\beta)}\sum_{\mu\nu}\bar{c}_{i\mu}\bar{c}_{i\nu}\chi_\mu(\mathbf{r})\chi_\nu(\mathbf{r}) \tag{11}$$

The SNO analysis is useful to identify those MOs that primarily contribute to the spin density at the nucleus.

3. COMPUTATIONAL DETAILS

The FC and SD terms were calculated using eqs 5 and 6, respectively. These formulas clearly show that the accuracy of HFCCs is essentially determined by that of the calculated spin density $\rho^{(\alpha-\beta)}(\mathbf{r})$ (eq 7). In the present work, the spin density was evaluated from the CAS-type wave functions. The active spaces used in this work are presented in Table 1. The DMRG code implemented by our group[70] was employed to obtain the active-space wave function for active space involving more than 16 orbitals; otherwise, the FCI procedure was used. The number of spin adapted renormalized states M was set to 512 in all DMRG calculations. We have implemented the spin adaptation of Zgid and Nooijen[67] in our DMRG code; therefore, the number of actual bases that are not spin adapted is much larger than M (approximately twice). The numerical convergence of HFCCs with respect to M will be discussed later (section 4.5).

For the diatomic radicals, the canonical HF-MOs were used as the initial orbitals. For vinyl radical, however, the initial orbitals were obtained from the restricted active space SCF (RASSCF) calculation including single and double excitations from RAS1 to RAS3 (singly occupied orbital was included in RAS2 space). The basis sets for this calculation are ANO-L[92,93] with 4s2p1d and 1s contractions for C and H atoms, respectively. The program package MOLCAS[94] was used for this purpose.

For comparison, the HFCCs were also calculated using the DFT and CCSD methods. The ORCA code[95] was used for DFT calculations with three functionals; the hybrid-GGA functional B3LYP, meta-GGA functional TPSS, and pure-GGA

functional BP.[96,97] The CCSD calculations were performed using the Gaussian 09 program package[98] without the frozen core approximation.

Table 2 shows the geometries of diatomic molecules used in these calculations, which were adopted from experimental measurements.[99] As a reference, these include the geometries employed in the previous work of Neese and colleagues.[38,47,100] The molecular structure of vinyl radical is shown Figure 1.

Table 2. Bond Lengths of $^2\Sigma$ Diatomic Radicals Used to Calculate the HFCCs

	bond length (Å)	
molecule	present work[a]	Neese et al.[b]
BO	1.2049	1.2049
CO^+	1.1500	1.1105
CN	1.1718	1.1555
AlO	1.6176	1.6176

[a]Ref 99. [b]Ref 100.

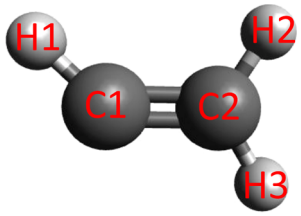

Figure 1. Molecular structure of vinyl (C_2H_3) radical.

Because not even an approximate experimental structure has been reported for this radical, we use the geometry theoretically recomended by Peterson and Dunning[101] as follows: r(C1C2) = 1.3102 Å, r(C1H1) = 1.0773 Å, r(C2H2) = 1.0830 Å, r(C2H3) = 1.0881 Å, a(C2C1H1) = 137.0°, a(H2C2C1) = 122.0°, a(H3C2C1) = 121.3°.

The point-group symmetry of molecules were assumed to be C_{2v} and C_s for diatomic and vinly radicals, respectively.

4. RESULTS AND DISCUSSION

4.1. BO and CO^+ Radicals. HFCC calculations were first performed for the BO and CO^+ radicals, which have been well characterized by the DFT and CC methods. The EPR-type basis sets reported by Barone and co-workers[102] in combination with appropriate functionals are known to generally provide reasonable HFCCs for organic radicals. On the other hand, the ANO-type basis sets by Roos and colleagues have been widely used for the construction of correlated molecular wave functions; however, the performance for HFCCs calculations has not yet been tested. Thus, the HFCCs of the BO and CO^+ radicals were evaluated here using both EPR-III and ANO-L-TZP basis sets. For the BO radical, the total number of AOs for the EPR-III and ANO-L-TZP basis sets is 69 and 60, respectively, while that for CO^+ is 80 and 60, respectively. The calculated values of the HFCCs are summarized in Tables 3 and 4. The experimental gas-phase and Ne-matrix HFCCs available for BO[103−106] and CO^+[107−109] are presented. The gas-phase and Ne-matrix values for the B center are not so different, while those for the C center differ significantly. The DFT/EPR-III and CCSD/EPR-III results for the BO radical are basically consistent with the previous results reported by Neese and co-workers,[38,47] while those for CO^+ are not. This inconsistency for CO^+ can be attributed to the difference in geometry used between the present and previous calculations, as shown in Table 2.

Fermi Contact Term. Herein, let this analysis focus on the HFCCs of less electronegative atom centers, that is, the B and C centers. The CCSD results with the EPR-III basis set for these centers are comparable with the experimental values and the errors with respect to the gas-phase values for the B and C centers are 1.37 and 3.44%, respectively. Among the DFT functionals, the B3LYP functional generally provides the best results. The BP and TPSS functionals yield FC terms for the B center that are in good agreement with the experimental results, while those for the C center are largely underestimated.

We now move to the results of the CASCI and CASSCF calculations. For the CASCI calculations, the effect of core correlation seems to be negligible, and the FC term is significantly decreased for both the B and C centers with enlargement of the active space, which results in underestimation with the DMRG-CASCI calculations. The CASSCF results clearly show that the active space with full valence shells alone is insufficient for reliable prediction of the HFCCs. In the presence of the polarization shell but without core correlation, the orbital optimization in the CASSCF calculations provides only a marginal improvement upon the CASCI results. In contrast, the FC term is significantly increased when the core correlation is taken into account. The FC term obtained by DMRG-CASSCF(13e,30o)/EPR-III is in excellent agreement with the experimental gas-phase values and the errors for the B and C centers are 0.87 and 0.99%, respectively.

Concerning the basis set, the values for the FC terms obtained with ANO-L-TZP are far from experimental values. This inadequacy of ANO-L-TZP for HFCC prediction is associated with contraction of the ANO-type basis sets, which are too contracted in the *s*-shells, and a similar argument was made regarding Dunning's correlation-consistent basis sets in ref 48. Thus, the ANO-type basis set is not sufficiently flexible to properly describe the spin-polarization of the core region. To confirm that the EPR-III basis set provides convergent basis set descriptions, HFCC calculations were performed with the uncontracted ANO-L-TZP basis set (Table 5). The total number of AOs for this uncontracted basis set is 164 for both BO and CO^+ radicals, which indicates that it is much larger and more flexible than the EPR-III basis set. Table 5 shows that the HFCC values obtained with the EPR-III and uncontracted ANO-L-TZP basis sets are comparable; therefore, it can be concluded that the basis set error in EPR-III is negligible for these $^2\Sigma$ radicals.

The spin density at the nuclear centers was analyzed using SNOs to determine the dependence of the FC term on the active space and the orbital optimization in more detail. Table 6 shows the contributions to the total spin density from the SNO with the largest spin occupation number (SON) and from the other SNOs at each of the B and C centers obtained with the EPR-III basis set. The eigenvector elements U_{ip} for construction of the SNO with the largest SON reveal that it is dominantly composed of a singly occupied MO (SOMO) and is thus regarded as a singly occupied SNO (SOSNO). The total spin density at the nuclei centers is dominated by the SOSNO because the remaining SNOs have negligible spin occupancies. For the CASCI calculation, enlargement of the active space depresses the net spin density associated with the SOSNO. The contribution from the SNOs, other than the

Table 3. HFCCs (in MHz) for the ^{2}BO Molecule Obtained with the EPR-III and ANO-L-TZP basis Sets, Where the Total Numbers of AOs are 69 and 60, Respectively

	^{11}B				^{17}O			
method	$A^{(K;c)}$	$A_{11}^{(K;d)}$	$A_{22}^{(K;d)}$	$A_{33}^{(K;d)}$	$A^{(K;c)}$	$A_{11}^{(K;d)}$	$A_{22}^{(K;d)}$	$A_{33}^{(K;d)}$
			EPR-III					
CASCI(9e,8o)	966.29	−28.11	−28.11	56.23	−23.72	12.28	12.28	−24.55
CASCI(9e,16o)	920.81	−25.29	−25.29	50.58	−12.08	16.95	16.95	−33.90
DMRG-CASCI(9e,28o)	903.81	−24.98	−24.98	49.97	−2.43	18.84	18.84	−37.69
DMRG-CASCI(13e,30o)	904.59	−25.02	−25.02	50.04	−2.94	18.83	18.83	−37.66
CASSCF(9e,8o)	916.85	−26.72	−26.72	53.44	−19.02	19.80	19.80	−39.60
DMRG-CASSCF(9e,28o)	912.09	−24.22	−24.22	48.44	−5.67	21.07	21.07	−42.14
DMRG-CASSCF(13e,30o)	1018.33	−24.44	−24.44	48.87	−11.95	20.84	20.85	−41.70
B3LYP	1074.79	−27.80	−27.80	55.60	−11.66	21.42	21.42	−42.83
TPSS	990.76	−27.04	−27.04	54.07	−5.70	25.20	25.20	−50.39
BP	989.79	−26.84	−26.84	53.68	−7.73	23.32	23.32	−46.64
CCSD	1041.15	−24.87	−24.87	49.75	−11.96	21.68	21.68	−43.36
			ANO-L-TZP					
CASCI(9e,8o)	969.42	−28.44	−28.44	56.88	−39.44	8.93	8.93	−17.87
CASCI(9e,16o)	911.81	−24.76	−24.76	49.53	−26.30	17.60	17.60	−35.21
DMRG-CASCI(9e,28o)	885.48	−23.13	−23.13	46.27	−32.44	19.43	19.43	−38.86
DMRG-CASCI(13e,30o)	901.80	−23.19	−23.19	46.38	−30.06	19.44	19.44	−38.87
FCI-CASSCF(9e,8o)	895.24	−25.86	−25.86	51.71	−31.70	19.95	19.95	−39.90
DMRG-CASSCF(9e,28o)	901.54	−23.33	−23.33	46.66	−24.07	20.89	20.90	−41.79
DMRG-CASSCF(13e,30o)	930.68	−23.55	−23.55	47.09	−24.58	20.92	20.93	−41.85
B3LYP	1015.79	−25.90	−25.90	51.80	−32.21	21.82	21.82	−43.64
TPSS	928.40	−25.30	−25.30	50.61	−22.84	25.47	25.47	−50.94
BP	929.68	−24.95	−24.95	49.89	−25.27	23.73	23.73	−47.45
CCSD	958.07	−23.52	−23.52	47.03	−30.58	21.88	21.88	−43.76
expt − gas phase[a]	1027	−27	−27	54			n/a	
expt − Ne matrix[b]	1033	−25	−25	50	−19	12	12	−24

[a]Ref 103. [b]Refs 104−106.

SOSNO, to the spin density is relatively very small. The total spin density thus decreases with enlargement of the active space, which leads to a decrease in the values of the FC terms for the B and C centers. From a comparison of the results from the DMRG-CASCI(9e,28o) and DMRG-CASCI(13e,30o) calculations, that is, with and without two 1s orbitals in CAS, it was concluded that the core correlation does not induce any significant change in the total spin density with the CASCI calculation.

Let us discus the orbital optimization effects on the spin density that arise from the CASSCF procedure. A comparison is made between two large CAS calculations: DMRG-CASSCF(9e,28o) and DMRG-CASSCF(13e,30o). The spin density associated with the SOSNO from the two DMRG-CASSCF calculations is similar, whereas that with the other SNOs significantly increases with inclusion of the two 1s orbitals in the CAS method. This indicates that the core correlation leads to strong enhancement of the total spin densities at nuclei centers. The poor agreement of DMRG-CASSCF(9e,28o) with the experiment data was significantly improved with DMRG-CASSCF(13e,30o).

Finally, we briefly discuss the FC term for the O center. The HFCCs of an electronegative atom is difficult to experimentally measure in the gas-phase; therefore, the calculation results are compared with Ne-matrix measurements. The errors of the DMRG-CASSCF(13e,30o)/EPR-III results relative to the experimental values are 7.04 and 13.60% for the O center in the BO and CO^+ radicals, respectively. The results obtained with CCSD are very close to those with DMRG-CASSCF-(13e,30o), especially for the EPR-III basis set.

Spin-Dipole Term. The elements of SD tensors are shown in Tables 3 and 4 for the B and C centers, respectively. The general conclusion is that the SD term is less dependent on the basis set and the active space than the FC term. The SD term converges smoothly with enlargement of the active space. The core correlation does not affect the SD term. With enlargement of the active space, the values of the SD term for the B and C centers decrease, while those for the O center increase for both radicals. The CCSD results are generally close to those obtained with DMRG-CASSCF(13e,30o). For the B center, the error of the SD term calculated by DMRG-CASSCF(13e,30o)/EPR-III with respect to that from Ne-matrix measurements (2.24%) is smaller than that from gas-phase measurements (9.48%). In contrast, the DMRG-CASSCF(13e,30o)/EPR-III results for the C center are in better agreement with the gas-phase value (2.56% error) than with the Ne-matrix value (8.53% error). Unfortunately, all the methods presented herein are largely overestimated with respect to the Ne-matrix values for the O centers in both radicals.

To summarize, the performance of the DMRG method for the prediction of HFCCs for BO and CO^+ radicals, which can be accurately described by DFT and CC methods, was assessed. While the DMRG-CASCI calculations gave results that were in poor agreement with the experimental values, the DMRG-CASCSCF calculations with orbital optimization and inclusion of the core correlation were in excellent agreement with the gas-phase measurements for the FC terms of the less electronegative centers.

4.2. CN Radical. Momose et al.[17] first used the SAC-CI method to calculate the HFCCs of the CN radical and the

Table 4. HFCCs (in MHz) for the $^2CO^+$ Molecule Obtained with the EPR-III and ANO-L-TZP Basis Sets, Where the Total Numbers of AOs are 80 and 60, Respectively

	^{13}C				^{17}O			
method	$A^{(K;c)}$	$A_{11}^{(K;d)}$	$A_{22}^{(K;d)}$	$A_{33}^{(K;d)}$	$A^{(K;c)}$	$A_{11}^{(K;d)}$	$A_{22}^{(K;d)}$	$A_{33}^{(K;d)}$
EPR-III								
CASCI(9e,8o)	1469.96	−48.44	−48.44	96.88	−7.87	29.14	29.14	−58.28
CASCI(9e,16o)	1450.21	−47.84	−47.84	95.68	1.84	30.24	30.24	−60.49
DMRG-CASCI(9e,28o)	1410.98	−47.68	−47.40	95.08	19.88	33.77	34.06	−67.83
DMRG-CASCI(13e,30o)	1409.23	−47.72	−47.46	95.17	20.01	33.78	34.04	−67.82
CASSCF(9e,8o)	1431.59	−46.13	−46.13	92.25	25.37	38.00	38.00	−76.00
DMRG-CASSCF(9e,28o)	1396.59	−44.14	−44.14	88.28	26.56	38.73	38.74	−77.46
DMRG-CASSCF(13e,30o)	1492.96	−44.82	−44.36	89.18	32.60	38.55	38.77	−77.31
B3LYP	1548.21	−50.08	−50.08	100.16	39.73	44.02	44.02	−88.04
TPSS	1444.78	−49.26	−49.26	98.52	39.73	47.10	47.10	−94.21
BP	1439.34	−50.22	−50.22	100.43	37.39	44.44	44.44	−88.88
CCSD	1557.75	−43.63	−43.63	87.26	32.87	42.78	42.78	−85.57
ANO-L-TZP								
CASCI(9e,8o)	1396.95	−47.39	−47.39	94.78	−10.88	29.19	29.19	−58.37
CASCI(9e,16o)	1365.90	−46.27	−46.27	92.54	4.55	31.85	31.85	−63.69
DMRG-CASCI(9e,28o)	1314.59	−45.99	−45.99	91.97	32.98	35.64	35.64	−71.28
DMRG-CASCI(13e,30o)	1296.20	−46.11	−46.11	92.22	32.12	35.61	35.61	−71.22
CASSCF(9e,8o)	1360.59	−45.29	−45.29	90.58	19.66	37.76	37.76	−75.51
DMRG-CASSCF(9e,28o)	1318.98	−43.48	−43.48	86.96	14.57	38.44	38.45	−76.89
DMRG-CASSCF(13e,30o)	1348.58	−43.72	−43.71	87.43	20.24	38.31	38.32	−76.64
B3LYP	1435.01	−47.80	−47.80	95.59	29.27	43.71	43.71	−87.43
TPSS	1331.67	−47.07	−47.07	94.14	31.79	46.71	46.71	−93.42
BP	1338.13	−47.88	−47.88	95.76	29.49	44.06	44.06	−88.11
CCSD	1425.84	−42.03	−42.03	84.05	18.53	42.30	42.30	−84.60
expt − gas phase	1506	−46	−46	92			n/a	
expt − Ne matrix[b]	1573	−49	−49	98	19	33	33	−66

[a]Ref 107. [b]Refs 108 and 109.

Table 5. HFCCs (in MHz) for the B Center in ^2BO and the C Center in $^2CO^+$ Radicals with the Uncontracted ANO-L Basis Set, Where the Total Number of AOs is 164 for Both Radicals

center	method	$A^{(K;c)}$	$A_{11}^{(K;d)}$
B in BO	B3LYP	1072.80	−28.16
	TPSS	982.71	−27.53
	BP	986.66	−27.47
	CCSD	1041.70	−25.28
	DMRG-CASSCF(13e,30o)	1028.41	−24.34
C in CO^+	B3LYP	1542.81	−50.38
	TPSS	1430.26	−49.61
	BP	1432.74	−50.77
	CCSD	1554.42	−43.85
	DMRG-CASSCF(13e,30o)	1493.89	−44.22

Table 6. SNO Contributions to Spin Density (in au) at the B (BO) and C (CO^+) Centers[a]

center	method	contribution of SOSNO	sum of the other SNO contributions	total
B	CASCI(9e,8o)	0.6722 (0.9870)	0.0012	0.6734
	CASCI(9e,16o)	0.6325 (0.9716)	0.0089	0.6414
	DMRG-CASCI(9e,28o)	0.6209 (0.9693)	0.0086	0.6295
	DMRG-CASCI(13e,30o)	0.6291 (0.9694)	0.0011	0.6302
	DMRG-CASSCF(9e,28o)	0.6238 (0.9700)	0.0120	0.6358
	DMRG-CASSCF(13e,30o)	0.6213 (0.9725)	0.0880	0.7097
C	CASCI(9e,8o)	1.2892 (0.9577)	0.0120	1.3076
	CASCI(9e,16o)	1.2664 (0.9553)	0.0236	1.2900
	DMRG-CASCI(9e,28o)	1.2394 (0.9529)	0.0157	1.2551
	DMRG-CASCI(13e,30o)	1.2398 (0.9530)	0.0139	1.2537
	DMRG-CASSCF(9e,28o)	1.2127 (0.9509)	0.0297	1.2424
	DMRG-CASSCF(13e,30o)	1.2385 (0.9525)	0.0942	1.3334

[a]The values in parentheses indicate the SON of SOSNO. For the CASSCF calculations, only the two largest active spaces are compared. Only the results of the EPR-III basis set are presented.

results compared favorably with the experimental results. However, as shown later by Fernandez et al.,[18] this agreement was fortuitous and resulted from cancellation of the basis set and correlation errors. These authors employed the multiconfiguration self-consistent-field (MCSCF) restricted-unrestricted (RU) response function method[110] to evaluate HFCCs for the CN radical. In this approach, although the spin polarization of the core orbitals cannot be described by the MCSCF wave function itself, it was perturbatively addressed by the response term. Accurate HFCCs for the CN radical were generally obtained with an appropriate conjunction between the active space and basis set. Gauld et al.[36] found that the QCISD approach with perturbative triples [QCISD(T)] underestimated the FC term of this radical. Nevertheless, good agreement with the experimental value was obtained when the CCSD(T) method was employed in place of

dx.doi.org/10.1021/ct400978j | J. Chem. Theory Comput. 2014, 10, 1953−1967

Table 7. HFCCs (in MHz) for the ^{2}CN Molecule Obtained with EPR-III Basis Set, Where the Total Number of AOs is 80[a]

	^{13}C				^{14}N			
method	$A^{(K;c)}$	$A_{11}^{(K;d)}$	$A_{22}^{(K;d)}$	$A_{33}^{(K;d)}$	$A^{(K;c)}$	$A_{11}^{(K;d)}$	$A_{22}^{(K;d)}$	$A_{33}^{(K;d)}$
CASCI(9e,8o)	936.03	−62.25	−62.25	124.51	8.78	−8.78	−8.78	17.55
CASCI(9e,16o)	767.11	−53.93	−53.93	107.85	3.70	−13.63	−13.63	27.27
DMRG-CASCI(9e,28o)	700.91	−54.34	−54.34	108.69	9.04	−15.51	−15.51	31.02
DMRG-CASCI(13e,30o)	685.66	−54.37	−54.37	108.74	8.18	−15.52	−15.52	31.04
CASSCF(9e,8o)	629.40	−51.06	−51.06	102.12	−19.72	−17.90	−17.90	35.81
DMRG-CASSCF(9e,28o)	596.48	−52.33	−52.32	104.66	−3.42	−19.22	−19.22	38.44
DMRG-CASSCF(13e,30o)	561.95	−52.92	−52.90	105.82	−20.14	−19.28	−19.27	38.55
B3LYP	572.62	−59.93	−59.93	119.86	−18.90	−21.66	−21.66	43.31
TPSS	504.83	−59.34	−59.34	118.68	−16.35	−22.12	−22.12	44.25
BP	494.08	−59.47	−59.47	118.94	−13.65	−21.58	−21.58	43.16
CCSD[b]	655.27	−52.97	−52.97	105.94	−20.03	−19.84	−19.84	39.68
CCSD[c]	655.40	−53.00	−53.00	106.00	−20.00	−19.80	−19.80	39.70
CCSD(T)[c]	556.10	−56.70	−56.70	113.50	−18.30	−19.10	−19.10	38.30
expt − Ar matrix[d]	588	−45	−45	90	−13	−15	−15	30

[a]For comparison, the CCSD and CCSD(T) results from Kossmann and Neese's work were also adopted, where the same basis set was used, but with a slightly different geometry (see Table 2). [b]Present work. [c]Kossmann and Neese, ref 38. [d]Ref 111.

QCISD(T). Neese and colleagues[47] recently reported that the double hybrid functional B2PLYP does not accurately characterize the HFCCs of the CN radical. In their later work,[38] while OO-MP2 methods provided the HFCCs in acceptable agreement with the experimental values for many molecules, it failed for the CN radical. From the previous subsection, the ANO-L-TZP basis set was deemed inadequate for HFCC prediction, so that only the results obtained with the EPR-III basis set were presented. The total number of AOs is 80. All results are summarized in Table7. Experimental gas-phase values for the CN radical are not available; therefore, Ne-matrix values[111] were used as references. The CCSD results of the present work are consistent with those reported by Kossmann and Neese,[38] where the same basis set (EPR-III), but different geometry, was used (see Table 2). Based on this consistency, we also adopted their CCSD(T) results[38] for further consideration.

Fermi Contact Term. Here, we mainly focus on the less electronegative center, that is, the C center. For the DFT calculations, the TPSS and BP functionals largely underestimate the FC term for the C center with errors of 14.29 and 15.99%, respectively. For the CC methods, CCSD overestimates the FC term for the C center with errors of up to 11.39%. However, with inclusion of the perturbative triples, the error is decreased to 5.43%.

Regarding the CASCI calculations, the FC term for the C center is rapidly decreased with enlargement of the active space. As the active space is extended from CAS(9e,28o) to CAS(13e,30o), the error is decreased from 19.20 to 16.60%. For the DMRG-CASSCF calculations, the FC term also converges smoothly with respect to the active space. By relaxing the orbitals with 1s orbitals in the active space, the error with respect to the experimental value is reduced to 4.43%. It is worth noting that the CCSD(T) and DMRG-CASSCF(13e,30o) results are very close together. This means that the DMRG-CASSCF(13e,30o) has captured the high-order correlation, which is required for the accuracy of the FC term for the C center in the CN radical.

The SNO contributions to the total spin density are analyzed next. Table 8 shows the SOSNO contribution and the summation of the other SNO contributions to the total spin density at the C center. The SOSNO spin density rapidly decreases with enlargement of the active space in the CASCI calculations, while the increase in the summation of the other SNO spin densities is relatively slow. Consequently, the total spin density at the C center decreases. For the CASSCF calculations, the orbital relaxation lowers the SOSNO spin density relative to that of the CASCI calculations. While the SOSNO spin densities from the DMRG-CASSCF(9e,28o) and DMRG-CASSCF(13e,30o) calculations are comparable, the summation of the other SNO spin densities from the latter is much smaller than from the former. Therefore, in contrast to the BO and CO^+ radicals, the core correlation in the CN radical reduces the summation of the other SNO spin densities.

Table 8. SNO Contributions to Spin Density (in au) at the C Center in the CN Radical[a]

method	contribution of SOSNO	sum of the other SNO contributions	total
CASCI(9e,8o)	0.8223 (0.9948)	0.0103	0.8326
CASCI(9e,16o)	0.6373 (0.9501)	0.0480	0.6823
DMRG-CASCI(9e,28o)	0.5312 (0.9439)	0.0922	0.6235
DMRG-CASCI(13e,30o)	0.5278 (0.9440)	0.0822	0.6099
DMRG-CASSCF(9e,28o)	0.4706 (0.9364)	0.0604	0.5310
DMRG-CASSCF(13e,30o)	0.4800 (0.9372)	0.0194	0.4996

[a]The values in parentheses indicate the SON of SOSNO. For the CASSCF calculations, only the two largest active spaces are compared.

We also provide a brief comment here with regard to the FC term for the N center. For the CASCI calculations, the FC term of the N center is completely wrong, even the sign, and this remains unchanged with changes in the active space. Although the DMRG-CASSCF(9e,28o) calculation can give the correct sign of the FC term, the error of the result with respect to the experimental value is very large at 76.92%. The DMRG-CASSCF(13e,30o) calculation improves the FC term to some degree, but the value is still far from the experimental result with an error of up to 54.92%. In addition, the CC results are very close to that obtained with the DMRG-CASSCF(13e,30o) calculation.

Table 9. HFCCs (in MHz) for the ^{2}AlO Molecule[a]

	^{27}Al				^{17}O			
method	$A^{(K;c)}$	$A_{11}^{(K;d)}$	$A_{22}^{(K;d)}$	$A_{33}^{(K;d)}$	$A^{(K;c)}$	$A_{11}^{(K;d)}$	$A_{22}^{(K;d)}$	$A_{33}^{(K;d)}$
CASCI(9e,8o)	830.31	−47.94	−47.94	95.89	9.56	36.41	36.41	−72.81
CASCI(9e,16o)	765.57	−48.32	−48.32	96.64	3.81	38.77	38.77	−77.54
DMRG-CASCI(9e,21o)	727.98	−47.31	−47.31	94.63	−0.71	42.56	42.56	−85.13
DMRG-CASCI(15e,28o)	670.79	−46.37	−46.36	92.73	−2.07	45.64	45.64	−91.28
DMRG-CASCI(21e,31o)	682.79	−46.39	−46.40	92.79	1.57	45.48	45.48	−90.95
DMRG-CASCI(15e,33o)	702.80	−46.41	−46.42	92.83	−3.16	45.26	45.25	−90.51
DMRG-CASCI(21e,36o)	708.32	−46.49	−46.50	92.99	1.61	45.13	45.15	−90.28
CASSCF(9e,8o)	830.07	−47.63	−47.63	95.26	−1.27	37.30	37.30	−74.60
DMRG-CASSCF(15e,28o)	629.25	−53.07	−53.20	106.27	−42.28	49.16	49.24	−98.40
DMRG-CASSCF(21e,31o)	887.02	−54.58	−51.39	105.97	−28.35	46.48	46.46	−92.94
DMRG-CASSCF(15e,33o)	573.08	−54.74	−54.88	109.62	−57.34	55.55	55.54	111.09
DMRG-CASSCF(21e,36o)	712.65	−54.04	−54.27	108.31	−35.04	52.21	52.19	−104.40
B3LYP	512.21	−59.97	−59.97	119.93	8.17	66.22	66.22	−132.43
TPSS	656.79	−56.10	−56.10	112.21	9.52	59.91	59.91	−119.83
BP	653.71	−56.86	−56.86	113.72	14.21	59.60	59.60	−119.20
CCSD[b]	482.02	−57.13	−57.13	114.26	18.14	63.86	63.86	−127.71
CCSD[c]	482.40	−57.20	−57.20	114.30	18.10	63.80	63.80	−127.70
CCSD(T)[c]	565.30	−56.20	−56.20	112.40	19.30	58.90	58.90	−117.80
expt − gas phase[d]	738	−56	−56	112			n/a	
expt − Ne matrix[e]	766	−52	−52	104	2	50	50	−100

[a]The IGLO-III and EPR-III basis sets were used for Al and O, respectively. The total number of AOs is 84. For comparison, the CCSD and CCSD(T) results from Kossmann and Neese's work were also adopted, where the same basis sets and geometry were used (see Table 2). [b]Present work. [c]Kossmann and Neese, ref 38. [d]Ref 113. [e]Ref 112.

Spin-Dipole Term. The calculated SD terms are also presented in Table 7. For the DFT calculations, all three functionals largely overestimate the SD terms for both the C and N centers, with errors of approximately 33.00 and 47.00%, respectively. For the CC calculations, the SD term for the C center calculated by CCSD appears better than that calculated by CCSD(T), where the errors are 17.78 and 26.00%, respectively. The SD term for the N center calculated by CCSD and CCSD(T) were comparable and the error with respect to the experimental data is approximately 32.00%. For the CASCI calculations, the SD terms for the C and N centers converge smoothly with respect to the active space and the core correlation does not affect the SD terms; the SD term for the C center increases with enlargement of the active space, while that for the N center decreases. Finally, the errors of the SD terms calculated by DMRG-CASSCF(13e,30o) relative to the experimental values were similar to those obtained by the CCSD calculations.

4.3. AlO Radical. The electronic structure of the AlO radical is determined by the transition of the ionic states that result from the large difference in the electronegativities of the atoms. The AlO radical is best characterized as somewhere between $Al^{2+}O^{2-}$ with the unpaired electron in the Al s orbital and $Al^{+}O^{-}$ with the unpaired electron in the O sp hybrid orbital polarized away from the metal. Therefore, the spin density will be extremely sensitive to the balance in the treatment of these two configurations. This leads to the difficulties in the measurement of the **A** tensor for AlO, both experimentally and by theoretical calculation. Electronic polarization in the AlO radical can easily arise in the matrix environment during experimental measurement. Knight and Weltner[112] reported the experimental FC terms for the Al center as 766, 899, and 920 MHz in Ne, Ar, and Kr matrices, respectively. Yamada et al.[113] later reported the experimental gas-phase value to be 738 MHz. The value for the Ne matrix is thus closest to the gas-phase value. The experimental dielectric constants of Ne, Ar, and Kr matrices are 1.10, 1.75, and 1.85, respectively; therefore, the FC term for the Al center increases with the dielectric constant of the matrix. According to Grein's theoretical explanation,[88,89] the large values for the FC term in Ar and Kr matrices result from the dominance of the $Al^{2+}O^{2-}$ configuration, which enhances the spin density at the Al center. Knight et al.[105] first used the CI method with the Dunning's double-ζ with polarizations (DZP) basis set to evaluate the FC term for Al in AlO, and the result was in reasonable agreement with the experimental values. However, in a later work, CI calculations using much larger uncontracted and contracted basis sets gave completely incorrect values.[87] These authors also determined that the MRCI-SD was not very effective to accurately characterize the HFCCs for the AlO radical. Although DFT calculations can give a qualitatively correct FC term for Al, the experimental agreement was still far from perfect.[47,87] Recently, the OO-MP2 and CC methods were also employed by Kossmann and Neese.[38] However, none of these methods provided results that are comparable to the experimental values, even for CCSD(T); the OO-MP2 results were too high, while the CC counterparts were too low. It is generally desirable to have the wave function provide appropriate mixing of the $Al^{+}O^{-}$ and $Al^{2+}O^{2-}$ configurations; therefore, the AlO radical is a multireference case.[90] It is thus interesting to assess the performance of the DMRG method for the evaluation of the **A** tensor for the AlO radical. We have used the IGLO-III[114] and EPR-III basis sets for Al and O, respectively. The total number of AOs is 84 and the results are summarized in Table 9. For comparison, this table also includes the experimental data of recent gas-phase[113] and Ne-matrix[112] measurements as well as the CCSD and CCSD(T) results from Kossmann and Neese,[38] where the same basis sets and geometry were used.

dx.doi.org/10.1021/ct400978j | J. Chem. Theory Comput. 2014, 10, 1953−1967

Fermi Contact Term. For DFT calculations, the B3LYP functional enormously underestimates the FC term for the Al center. Although the other functionals reduce this underestimation, the error from the gas-phase value is still large at approximately 11.00%. The failure of CCSD has been confirmed with an error as large as 35.69%. The perturbative triples correction improved upon the CCSD result to some extent, but the result (error 23.40%) was still far from experimental values. The failure of CCSD(T) can be attributed to the multireference problem of the AlO radicals discussed previously.

For the DMRG calculations, inclusion of the 3d polarization shells is insufficient to achieve accuracy; therefore, the Al 4d polarization in active space was also included (see Table 1 for details). With the CASCI calculation, the FC term for the Al center was nonmonotonically dependent on the active spaces; as the size of the active space was increased, the FC term first decreased and then slowly increased. The result of the DMRG-CASCI(13e,36o) calculation (error 4.02%) is in reasonable agreement with the gas-phase value. For the CASSCF calculation, there is no improvement of the FC term calculated by CASCI if the CAS only consists of full valence shells. The FC term for the Al center is quite sensitive with further enlargement of the active space. The FC terms are too low without core correlation; however, the FC terms are too high with core correlation but without Al 4d polarization. Good agreement with the gas-phase value with an error of 3.43% was obtained when all these orbitals were included in the active space.

Table 10 presents the SNO contributions to the total spin density at the Al center. We only compare the spin densities calculated with the four largest active spaces. The CASCI results are considered first. The SOSNO spin density slowly increases with enlargement of the CAS, while the summation of the other SNO contribution seems to remain unchanged. The increase of total spin density then follows the increase of the SOSNO spin density. Although the SOSNO spin densities from the DMRG-CASCI calculations are generally comparable to the total spin density from the gas-phase measurement (0.634 au[113]), the calculated total spin densities are lowered by the negative contributions from the other SNOs, which leads to the underestimation of the DMRG-CASCI calculations. We now discuss the DMRG-CASSCF spin density. Without the core orbitals in the active space (i.e. CAS(15e,28o) and CAS(15e,33o)) the total spin densities are too low relative to the gas-phase value, due to the largely negative contributions of the other SNOs. In contrast, the total spin density from the DMRG-CASSCF(21e,31o) calculation is too high relative to the gas-phase value, as a result of the high SOSNO spin density. When the core orbitals and Al 4d polarization shell are taken into account (i.e. CAS(21e,36o)), the SOSNO spin density is close to the gas-phase value and the summation of other SNO contributions is relatively small. Consequently, the total spin density in this case is comparable to that of the gas-phase measurement.

Table 10. SNO Contributions to Spin Density (in au) at the Al Center in the AlO Radical[a]

method	contribution of SOSNO	sum of the other SNO contributions	total
DMRG-CASCI(15e,28o)	0.6191 (0.9262)	−0.0436	0.5754
DMRG-CASCI(21e,31o)	0.6236 (0.9264)	−0.0385	0.5850
DMRG-CASCI(15e,33o)	0.6459 (0.9292)	−0.0430	0.6029
DMRG-CASCI(21e,36o)	0.6513 (0.9306)	−0.0436	0.6076
DMRG-CASSCF(15e,28o)	0.6491 (0.9331)	−0.1095	0.5396
DMRG-CASSCF(21e,31o)	0.7296 (0.9625)	0.0312	0.7609
DMRG-CASSCF(15e,33o)	0.5710 (0.9376)	−0.0794	0.4915
DMRG-CASSCF(21e,36o)	0.6259 (0.9482)	−0.0146	0.6113

[a]The values in parentheses indicate the SON of SOSNO. Only the four largest active spaces are compared.

Figure 2 presents the spatial distribution of the SOSNO spin density for the AlO radical. The largest CAS (i.e. CAS-(21e,36o)) provides an FC term for the Al center that is in excellent agreement with the gas-phase value, and the spatial distribution has peaks with medium height. In the presence of 4d polarization but without core correlation (i.e. CAS-(15e,33o)) the distribution plot has the highest peaks around the O center, while the peak at the Al center is the lowest. The features are opposite for the case of CAS(21e,31o). This figure indicates that the difference in the SOSNO spin density between CAS(15e,33o) and CAS(21e,36o) is smaller than that between CAS(21e,31o) and CAS(21e,36o), which implies that the SOSNO spin density is more significantly affected by the polarization shell than by the core correlation.

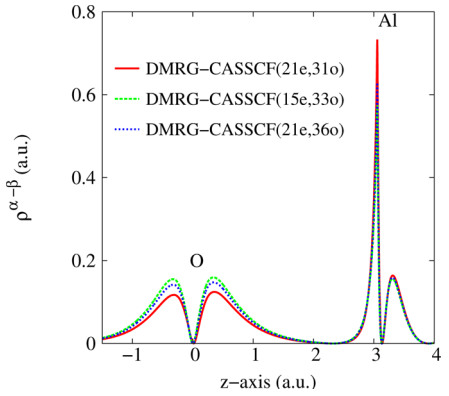

Figure 2. Spin density distribution of SOSNO for the AlO radical. The geometry of the AlO radical (in au) is O(0.000, 0.000, 0.000) and Al(0.000, 0.000, 3.057). The results were calculated using the DMRG-CASSCF(15e,33o), DMRG-CASSCF(21e,31o), and DMRG-CASSCF(21e,36o) procedures.

Concerning the FC term for the O center, none of present methods except the DMRG-CASCI calculations can correctly reproduce the Ne-matrix value. However, the agreement of the DMRG-CASCI results with the Ne-matrix value can be attributed to fortuitous error cancellation. In addition, the results obtained by CC calculations are comparable to those obtained with the DMRG-CASSCF(21e,36o) calculation.

Spin-Dipole Term. We first discuss the SD term for the Al center. For the DFT calculations, the SD terms are very close to the gas-phase value when using the BP and TPSS functionals, while that with the B3LYP functional gave an overestimation with an error of 7.09%. Similarly, the SD term calculated by the CCSD method is comparable with the gas-phase value and has

dx.doi.org/10.1021/ct400978j | J. Chem. Theory Comput. 2014, 10, 1953−1967

Table 11. Fermi Contact Values (in MHz) of $^2A'$ state of C_2H_3 Radical Using EPR-III basis Set, Where the Total Number of AOs is 113

method	C1	C2	H1	H2	H3
DMRG-CASSCF(15e,33o)	311.21	−27.11	21.14	158.03	101.59
UHF	479.40	−116.56	−37.44	193.94	138.91
B3LYP	324.59	−12.05	55.29	173.55	112.14
TPSS	314.72	−17.59	60.97	181.30	109.47
BP	293.77	−9.38	49.06	173.69	112.57
CCSD	316.12	−16.90	39.00	157.13	96.83
expt.[a]	301.54	−24.10	38.67	184.80	110.97

[a]Taken from ref 117.

Table 12. Different in DMRG Energy As Well As Total Discarded Weight between Last Two DMRG Sweeps for DMRG-CASSCF Calculations with Largest Active Spaces for Each System Studied in This Work[a]

molecules	DMRG-CASSCF calculations	deviation of energies (mE_h)	deviation of total discarded weight	total discarded weight
BO	DMRG-CASSCF(13e,30o)	0.00143	6.96157×10^{-6}	3.69354×10^{-6}
CO^+	DMRG-CASSCF(13e,30o)	0.00066	7.77564×10^{-6}	4.65225×10^{-6}
CN	DMRG-CASSCF(13e,30o)	0.00132	1.36235×10^{-5}	8.14189×10^{-6}
AlO	DMRG-CASSCF(21e,36o)	0.00249	4.73789×10^{-5}	1.60101×10^{-5}
C_2H_3	DMRG-CASSCF(15e,33o)	0.00105	3.66949×10^{-5}	3.36053×10^{-5}

[a]The total discarded weight of last DMRG sweep is also included.

an error of 2.02%. For the DMRG calculation, the SD term for the Al center is less sensitive to the active space. All DMRG-CASCI calculations largely underestimate the SD term, where the errors relative to the gas-phase and Ne-matrix values are approximately 16.00% and 10.00%, respectively. Interestingly, all DMRG-CASSCF results fall between the gas-phase and Ne-matrix values. In the case of the O center, both DFT and CC approaches largely overestimate the Ne-matrix value with the largest error up to 32.44% (for the B3LYP functional). Similarly to the Al center, the SD term for the O center is underestimated by the DMRG-CASCI calculation. Finally, the result with DMRG-CASSCF(21e,36o) is very close to the Ne-matrix value with an error of 1.46%.

4.4. Vinyl Radical. In this subsection, we will consider the performance of DMRG method for Fermi contact prediction of vinyl radical. For the $^2A'$ ground state, the unpaired electron is located in the 8a′ orbital which is an in-plane sp hybrid. The vinyl radical, therefore, is designated as σ radical. Briefly, the FC values of vinyl radical have been previously evaluated using several conventional methods, such as DFT,[115] MR-SCI,[116] and CC.[117,118] In the present calculations, we have used the EPR-III basis set for both C and H atoms. The total number of AOs is 113. We herein focus on the FC term of C atoms; therefore, we included a large number of orbitals of C atoms in active space, while only 1s orbitals of H atoms were taken into account (see Table 1). It is difficult to properly chose active orbitals from HF orbitals for this molecule; therefore, we employed the orbitals obtained from RASSCF/ANO-L calculation (see section 3 for details) as the initial orbitals for DMRG calculations. Because we used different basis sets for preparing initial orbitals and DMRG calculation, we have not presented the DMRG-CASCI results. We also provided the DFT (B3LYP, TPSS, and BP functionals), UHF, as well as CCSD results for comparison. All results are summarized in Table 11.

We first discuss the FC terms of both C centers. It is obvious that the UHF method largely overestimates these FC terms. For three DFT calculations, while their results for C1 center are in reasonable agreement with experimental value, they significantly underestimate the FC term of C2 center with smallest and largest error of up to 27.01% (for TPSS functional) and 61.08% (for BP functional), respectively. The similar situation was observed for the CCSD calculation. The errors of CCSD results from experimental values are 4.84% and 29.88% for C1 and C2 centers, respectively. The DMRG-CASSCF(15e,33o) calculation provided the FC terms of both C centers in good agreement with experimental values. The errors are 3.21% and 12.49% for C1 and C2 centers, respectively.

We now discuss the FC terms of three H centers. Although all absolute values of HF results are reasonable, the sign of FC term of H1 center is different from that of experimental values. All the DFT calculations provide the FC terms of H2 and H3 centers in good agreement with experimental values; however, they overestimate the FC term of H1 center. In contrast to DFT, the CCSD method gives an accurate FC term for H1 center, while the FC terms for H2 and H3 centers of this method are far away from experimental values. The DMRG-CASSCF(15e,33o) calculation underestimates the FC terms of all H centers. The large discrepancy between DMRG results and experimental values seems to arise because we only included the H 1*s* orbital in active space. In order to get more accurate FC terms for H centers, we should include more orbitals of H atom in active space.

4.5. Accuracy of DMRG Method for HFCC Prediction. The quality of a DMRG wave function is dependent on the number of renormalized basis states *M*, and variationally converges to an exact description with increasing *M*. A more accurate DMRG wave function requires a larger *M*, which implies greater computational cost. Therefore, it is useful to reveal the convergence of HFCCs calculated by the DMRG method with respect to *M*.

Table 12 presents the differences in DMRG energy as well as total discarded weight between the last two DMRG sweeps in DMRG-CASSCF calculations with the largest active spaces for each system studied in this work. The total discarded weights of the last DMRG sweep is also provided. From this Table, we can see that the change in DMRG energy measured in the last two sweeps is negligible.

Let us illustrate the convergence of DMRG results with increasing calculation level. We have chosen the CN radical as an example for this purpose. DMRG calculations with M = 128, 256, and 1024 for CAS(13e,30o) were performed. The MOs from the DMRG-CASSCF(13e,30o) calculation with M = 512 was used as the orbital basis for the other calculations. To maintain consistence between the different DMRG calculations, the CASCI procedure was conducted with the same orbital basis. Table 13 presents the convergence of the total electronic energy, FC term, and SD term for the C center with respect to M. The energy with M = 512 is converged to 0.604 mE_h when compared to that of M = 1024. The FC term significantly decreases when going from M = 128 to 256 (approximately 13.00 MHz) and seems to be convergent with larger values of M. This situation also happens to the SD term.

Table 13. Total Discarded Weight, Total Energy, and HFCCs at the C Center at Different Number of Renormalized States M for CN Radical[a]

M	total discarded weight	energy (E_h)	FC term $A^{(K,c)}$ (MHz)	SD term $A_{11}^{(K,d)}$ (MHz)
128	1.16877×10^{-4}	−92.570835	576.80	−53.18
256	2.78911×10^{-5}	−92.575539	563.79	−52.97
512	8.14189×10^{-5}	−92.577510	561.95	−52.92
1024	1.35497×10^{-6}	−92.578114	559.44	−52.86
∞		−92.578276	558.99[b]	−52.85[b]

[a]Only the first element is presented for the SD term. The active space is CAS(13e,30o). The convergent MOs of the DMRG-CASSCF-(13e,30o) calculation with M = 512 were used as a reference for the other DMRG calculations and only the CASCI procedure was performed for these calculations. [b]Linear extrapolation from two points at M = 512 and 1024 of HFCCs vs the total discarded weight (see Figure 3).

In Figure 3, we plotted the total energy, FC term, and SD term vs the discarded weights at different values of M. We excluded the data with M = 128 for extrapolation. It is known that the least-squares fitting represents a near direct proportionality between the total energy and total discarded weight[64,70] as shown in upper panel of Figure 3. The extrapolation estimates the DMRG energy at M = ∞ to be $-92.578276E_h$; therefore, the DMRG energy at M = 512 (see Table 13) is found to be accurate to $0.766mE_h$. The HFCCs vs total discarded weight, however, are nonlinear as shown in the middle (FC term) and lower (SD term) panels of Figure 3. Although the number of points from available data is not sufficient to generally extrapolate the FC and SD terms at M = ∞, we have attempted to linearly extrapolate from last two points (at M = 512 and 1024). We then obtained the approximate estimations of the FC and SD terms at M = ∞ to be 558.99 and −52.85 MHz, respectively. Errors of FC and SD terms at M = 512 (see Table 13) from these approximate estimations are 0.53% and 0.13%, respectively.

Generally, due to the nonlinearity of HFCCs vs total discarded weight, it is not feasible to provide the general trend for convergence of HFCCs with respect to M. However, from the approximate estimation of HFCC values at M = ∞, we found that the results at M = 512 are reliable.

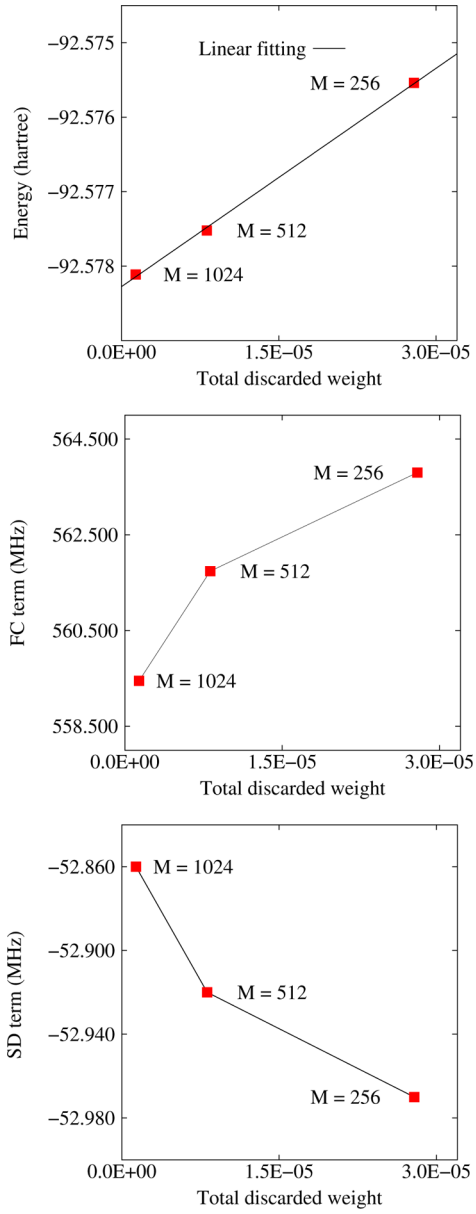

Figure 3. Total energy (upper panel), FC term (middle panel), and SD term (lower panel) vs the total discarded weight for DMRG calculations of CN radical at M = 256, 512, and 1024.

5. CONCLUSION AND OUTLOOK

In summary, DMRG calculations were performed to predict the HFCCs of 4 $^2\Sigma$ diatomic radicals (BO, CO^+, CN, and AlO) and vinyl (C_2H_3) radical. The HFCCs of the less electronegative centers (B, C, and Al) obtained were in excellent agreement with the experimental values. The present work not only provides some insight into the accuracy of HFCC predictions using the DMRG method, but also serves as the benchmark for further work. It should be emphasized that the DMRG algorithm used herein was considered as a near-FCI method and the electron correlation effects were systematically investigated using the CAS-type procedures (i.e., CASCI and CASSCF). At this point, we are able to answer the two questions addressed in the introduction. (i) Our assessment shows that the active space method has the potential to accurately describe the HFCCs, but the active space must be addressed by the construction of active orbitals. Generally, the

dx.doi.org/10.1021/ct400978j | J. Chem. Theory Comput. 2014, 10, 1953−1967

FC term is particularly sensitive to the choice of active space. Moreover, the DMRG method is also suitable to deal with multireference cases such as the AlO radical. (ii) It is necessary to correlate the core electrons to correctly obtain the spin density at the nucleus; therefore, the core orbitals should be included in CAS. At the same time, the inclusion of polarization shells is necessary to describe the dynamical correlation, which provides the appropriate spin-polarized effects.

Most CASCI calculations provided FC terms that were in poor agreement with the experimental values, while reasonably accurate results were obtained when the orbital optimization procedure was employed with the same CAS. This situation can be attributed to the nature of the one-particle basis in which the DMRG calculations were performed. The canonical HF orbitals were used as the orbital basis for the DMRG-CASCI calculation, whereas the DMRG calculation in conjunction with the CASSCF procedure was conducted with much more compact orbitals that were obtained through the orbital optimization procedure. The SD term is generally less sensitive to the level of theory, as well as the size of the active space, than the FC term. The SD terms calculated using the DMRG-CASSCF approach with the largest active spaces were better to some extent than those calculated using conventional methods in most cases.

The assessment for the convergence of HFCCs with respect to the number of renormalized states M was also performed. We found that the HFCCs vs total discarded weight did not yield a linear relation, while energies were in direct proportional to total discarded weights. Although Boguslawski et al.[83] has recently claimed that reliable reference spin densities can be obtained even if the total energies are not converged with respect to M, the conclusion for HFCCs, which are calculated from spin density, is questionable. This is because the nature of HFCCs is different from that of total spin density, especially the FC term, which is the direct numerical measure of spin density at the position of nucleus. Despite this fact, we have attempted to estimate the HFCCs at $M = \infty$ by linear extrapolation from two points at $M = 512$ and 1024. Errors of HFCCs at $M = 512$ from these approximate estimations are negligible for our test cases.

Finally, we have explored the reliability of the DMRG method for the HFCC prediction of diatomic radicals. For molecules with more complicated structure, the active space must be sufficiently large to capture the electron correlation effect, which implies expensive computation. Therefore, the combination of the DMRG method with another multireference dynamical correlation model is useful to obtain accurate HFCCs. To accurately predict the HFCCs of species that contain heavy elements requires consideration of the relativistic effects, including the scalar and spin−orbit coupling effects. Further work on these issues is in progress.

AUTHOR INFORMATION

Corresponding Author

*E-mail: lantran@ims.ac.jp

Notes

The authors declare no competing financial interest.

ACKNOWLEDGMENTS

The authors are grateful to Dr. Jakub Chalupský for valuable discussions. This research was supported in part by the Core Research for Grant-in-Aid for Scientific Research (C) (Grant No. 25410030) and (B) (Grant No. 25288013) from the Ministry of Education, Culture, Sports, Science, and Technology of Japan (MEXT). The generous support of computational resources from the Research Center of Computer Science (RCCS) at the Institute for Molecular Science (IMS) is acknowledged.

REFERENCES

(1) Van Vleck, J. *Rev. Mod. Phys.* **1951**, *23*, 213−227.
(2) Kutzelnigg, W. *Theo. Chim. Act.* **1988**, *73*, 173−200.
(3) Frosch, R. A.; Foley, H. *Phys. Rev.* **1952**, *88*, 1337−1349.
(4) Improta, R.; Barone, V. *Chem. Rev.* **2004**, *104*, 1231−1253.
(5) Hameka, H. F.; Turner, A. G. *J. Magn. Reson. (1969)* **1985**, *64*, 66−75.
(6) Nakatsuji, H.; Kato, H.; Yonezawa, T. *J. Chem. Phys.* **1969**, *51*, 3175−3180.
(7) Chipman, D. M. *Theo. Chim. Act.* **1992**, *82*, 93−115.
(8) Sekino, H.; Bartlett, R. J. *J. Chem. Phys.* **1985**, *82*, 4225−4228.
(9) Perera, S. A.; Watts, J. D.; Bartlett, R. J. *J. Chem. Phys.* **1994**, *100*, 1425−1432.
(10) Fau, S.; Bartlett, R. J. *J. Phys. Chem. A* **2003**, *107*, 6648−6655.
(11) Puzzarini, C.; Barone, V. *J. Chem. Phys.* **2008**, *129*, 084306−7.
(12) Puzzarini, C.; Barone, V. *Phys. Chem. Chem. Phys.* **2008**, *10*, 6991−6697.
(13) Puzzarini, C.; Barone, V. *J. Chem. Theory Comput.* **2009**, *5*, 2378−2387.
(14) Puzzarini, C.; Barone, V. *J. Chem. Phys.* **2010**, *133*, 184301−11.
(15) Barone, V.; Biczysko, M.; Bloino, J.; Egidi, F.; Puzzarini, C. *J. Chem. Phys.* **2013**, *138*, 234303−14.
(16) Momose, T.; Nakatsuji, H.; Shida, T. *J. Chem. Phys.* **1988**, *89*, 4185−4192.
(17) Momose, T.; Yamaguchi, M.; Shida, T. *J. Chem. Phys.* **1990**, *93*, 7284−7292.
(18) Fernández, B.; Jørgensen, P.; Simons, J. *J. Chem. Phys.* **1993**, *98*, 7012−7019.
(19) Engels, B. *Theo. Chim. Act.* **1993**, *86*, 429−437.
(20) Bauschlicher, C. W., Jr.; Langhoff, S. R.; Partridge, H.; Chong, D. P. *J. Chem. Phys.* **1988**, *89*, 2985−2992.
(21) Engels, B.; Peyerimhoff, S. *Z. Phys. D* **1989**, *13*, 335−343.
(22) Engels, B.; Peyerimhoff, S. D.; Davidson, E. *Mol. Phys.* **1987**, *62*, 109−127.
(23) Feller, D.; Davidson, E. R. *J. Chem. Phys.* **1988**, *88*, 7580−7587.
(24) Bauschlicher, C. W., Jr. *J. Chem. Phys.* **1990**, *92*, 518−521.
(25) Engels, B. *Chem. Phys. Lett.* **1991**, *179*, 398−404.
(26) Engels, B. *J. Chem. Phys.* **1994**, *100*, 1380−1386.
(27) Löwdin, P.-O. *J. Chem. Phys.* **1951**, *19*, 1396−1401.
(28) Nitzsche, L. E.; Davidson, E. R. *J. Chem. Phys.* **1978**, *68*, 3103−3109.
(29) Davidson, E. R.; McMurchie, L. E.; Day, S. J. *J. Chem. Phys.* **1981**, *74*, 5491−5496.
(30) Rawlings, D. C.; Davidson, E. R. *Chem. Phys. Lett.* **1983**, *98*, 424−427.
(31) Suter, H.; Engels, B. *J. Chem. Phys.* **1994**, *100*, 2936−2942.
(32) Suter, H.; Huang, M.-B.; Engels, B. *J. Chem. Phys.* **1994**, *101*, 7686−7691.
(33) Perić, M.; Engels, B. *J. Mol. Spectrosc.* **1995**, *174*, 334−352.
(34) Kristiansen, P.; Veseth, L. *J. Chem. Phys.* **1986**, *84*, 2711−2719.
(35) Kristiansen, P.; Veseth, L. *J. Chem. Phys.* **1986**, *84*, 6336−6343.
(36) Gauld, J. W.; Eriksson, L. A.; Radom, L. *J. Phys. Chem. A* **1997**, *101*, 1352−1359.
(37) Kaupp, M.; Arbuznikov, A. V.; Heßelmann, A.; Görling, A. *J. Chem. Phys.* **2010**, *132*, 184107−10.
(38) Kossmann, S.; Neese, F. *J. Phys. Chem. A* **2010**, *114*, 11768−11781.
(39) Eriksson, L. A.; Malkina, O. L.; Malkin, V. G.; Salahub, D. R. *J. Chem. Phys.* **1994**, *100*, 5066−5075.
(40) Munzarová, M.; Kaupp, M. *J. Phys. Chem. A* **1999**, *103*, 9966−9983.

(41) Munzarová, M. L.; Kubacek, P.; Kaupp, M. *J. Am. Chem. Soc.* **2000**, *122*, 11900−11913.
(42) Malkin, E.; Malkin, I.; Malkina, O. L.; Malkin, V. G.; Kaupp, M. *Phys. Chem. Chem. Phys.* **2006**, *8*, 4079−4085.
(43) Komorovskỳ, S.; Repiskỳ, M.; Malkina, O. L.; Malkin, V. G.; Malkin, I.; Kaupp, M. *J. Chem. Phys.* **2006**, *124*, 084108−8.
(44) Munzarová, M. L. In *Calculation of NMR and EPR Parameters*; Kaupp, M., Bühl, M., Malkin, V. G., Eds.; Wiley-VCH: Weinheim, Germany, 2006; pp 463−482.
(45) Remenyi, C.; Reviakine, R.; Kaupp, M. *J. Phys. Chem. A* **2006**, *110*, 4021−4033.
(46) Remenyi, C.; Reviakine, R.; Kaupp, M. *J Phys. Chem. B* **2007**, *111*, 8290−8304.
(47) Kossmann, S.; Kirchner, B.; Neese, F. *Mol. Phys.* **2007**, *105*, 2049−2071.
(48) Hedegård, E. D.; Kongsted, J.; Sauer, S. P. *J. Chem. Theory Comput.* **2011**, *7*, 4077−4087.
(49) Autschbach, J.; Patchkovskii, S.; Pritchard, B. *J. Chem. Theory Comput.* **2011**, *7*, 2175−2188.
(50) Aquino, F.; Pritchard, B.; Autschbach, J. *J. Chem. Theory Comput.* **2012**, *8*, 598−609.
(51) Verma, P.; Autschbach, J. *J. Chem. Theory Comput.* **2013**, *9*, 1932−1948.
(52) Lee, C.; Yang, W.; Parr, R. G. *Phys. Rev. B* **1988**, *37*, 785−789.
(53) Becke, A. D. *J. Chem. Phys.* **1993**, *98*, 5648−5652.
(54) Perdew, J. P.; Burke, K.; Ernzerhof, M. *Phys. Rev. Lett.* **1996**, *77*, 3865−3868.
(55) Perdew, J. P.; Burke, K.; Ernzerhof, M. *Phys. Rev. Lett.* **1997**, *78*, 1396−1396.
(56) Tao, J.; Perdew, J. P.; Staroverov, V. N.; Scuseria, G. E. *Phys. Rev. Lett.* **2003**, *91*, 146401−4.
(57) Grimme, S. *J. Chem. Phys.* **2006**, *124*, 034108−16.
(58) Engels, B. In *Calculation of NMR and EPR Parameters*; Kaupp, M., Bühl, M., Malkin, V. G., Eds.; Wiley-VCH: Weinheim, Germany, 2006; pp 483−492.
(59) White, S. R. *Phys. Rev. Lett.* **1992**, *69*, 2863−2866.
(60) White, S. R. *Phys. Rev. B* **1993**, *48*, 10345−10356.
(61) White, S. R.; Martin, R. L. *J. Chem. Phys.* **1999**, *110*, 4127−4130.
(62) Mitrushenkov, A. O.; Fano, G.; Ortolani, F.; Linguerri, R.; Palmieri, P. *J. Chem. Phys.* **2001**, *115*, 6815−6821.
(63) Chan, G. K.-L.; Head-Gordon, M. *J. Chem. Phys.* **2002**, *116*, 4462−4476.
(64) Chan, G. K.-L.; Head-Gordon, M. *J. Chem. Phys.* **2003**, *118*, 8551−8554.
(65) Legeza, Ö.; Röder, J.; Hess, B. A. *Phys. Rev. B* **2003**, *67*, 125114−10.
(66) Moritz, G.; Reiher, M. *J. Chem. Phys.* **2007**, *126*, 244109−16.
(67) Zgid, D.; Nooijen, M. *J. Chem. Phys.* **2008**, *128*, 014107−12.
(68) Zgid, D.; Nooijen, M. *J. Chem. Phys.* **2008**, *128*, 144116−11.
(69) Marti, K. H.; Ondík, I. M.; Moritz, G.; Reiher, M. *J. Chem. Phys.* **2008**, *128*, 014104−13.
(70) Kurashige, Y.; Yanai, T. *J. Chem. Phys.* **2009**, *130*, 234114−21.
(71) Ghosh, D.; Hachmann, J.; Yanai, T.; Chan, G. K. *J. Chem. Phys.* **2008**, *128*, 144117−14.
(72) Yanai, T.; Kurashige, Y.; Ghosh, D.; Chan, G. K. *Int. J. Quantum Chem.* **2009**, *109*, 2178−2190.
(73) Chan, G. K.-L.; Kállay, M.; Gauss, J. *J. Chem. Phys.* **2004**, *121*, 6110−6116.
(74) Chan, G. K.-L. *J. Chem. Phys.* **2004**, *120*, 3172−3178.
(75) Hachmann, J.; Cardoen, W.; Chan, G. K.-L. *J. Chem. Phys.* **2006**, *125*, 144101−12.
(76) Hachmann, J.; Dorando, J. J.; Avilés, M.; Chan, G. K.-L. *J. Chem. Phys.* **2007**, *127*, 134309−9.
(77) Yanai, T.; Kurashige, Y.; Neuscamman, E.; Chan, G. K.-L. *J. Chem. Phys.* **2010**, *132*, 024105−9.
(78) Kurashige, Y.; Yanai, T. *J. Chem. Phys.* **2011**, *135*, 094104−9.
(79) Kurashige, Y.; Chan, G. K.-L.; Yanai, T. *Nat. Chem.* **2013**, 660−666.
(80) Saitow, M.; Kurashige, Y.; Yanai, T. *J. Chem. Phys.* **2013**, *139*, 044118−15.
(81) Barcza, G.; Legeza, Ö.; Marti, K.; Reiher, M. *Phys. Rev. A* **2011**, *83*, 012508−15.
(82) Tecmer, P.; Boguslawski, K.; Legeza, Ö.; Reiher, M. *Phys. Chem. Chem. Phys.* **2014**, *16*, 719−727.
(83) Boguslawski, K.; Marti, K. H.; Legeza, Ö.; Reiher, M. *J. Chem. Theory Comput.* **2012**, *8*, 1970−1982.
(84) Legeza, Ö.; Sólyom, J. *Phys. Rev. B* **2003**, *68*, 195116−19.
(85) Legeza, Ö.; Sólyom, J. *Phys. Rev. B* **2004**, *70*, 205118−7.
(86) Lengsfield, B., III; Liu, B. *J. Chem. Phys.* **1982**, *77*, 6083−6089.
(87) Knight, L. B., Jr.; Kirk, T. J.; Herlong, J.; Kaup, J. G.; Davidson, E. *J. Chem. Phys.* **1997**, *107*, 7011−7019.
(88) Grein, F. *J. Phys. Chem. A* **2005**, *109*, 9270−9278.
(89) Grein, F. *Chem. Phys. Lett.* **2006**, *418*, 100−104.
(90) Gilka, N.; Tatchen, J.; Marian, C. *Chem. Phys.* **2008**, *343*, 258−269.
(91) Dupuis, M.; Rys, J.; King, H. F. *J. Chem. Phys.* **1976**, *65*, 111−116.
(92) Widmark, P.-O.; Malmqvist, P.-Å.; Roos, B. O. *Theo. Chim. Act.* **1990**, *77*, 291−306.
(93) Widmark, P.-O.; Persson, B. J.; Roos, B. O. *Theor. Chim. Act.* **1991**, *79*, 419−432.
(94) Karlström, G.; Lindh, R.; Malmqvist, P.-Å.; Roos, B. O.; Ryde, U.; Veryazov, V.; Widmark, P.-O.; Cossi, M.; Schimmelpfennig, B.; Neogrady, P.; Seijo, L. *Comput. Mater. Sci.* **2003**, *28*, 222−239.
(95) Neese, F. *WIREs: Comp. Mol. Sci.* **2012**, *2*, 73−78.
(96) Becke, A. D. *Phys. Rev. A* **1988**, *38*, 3098−3100.
(97) Perdew, J. P. *Phys. Rev. B* **1986**, *33*, 8822−8824.
(98) Frisch, M. J.; Trucks, G. W.; Schlegel, H. B.; Scuseria, G. E.; Robb, M. A.; Cheeseman, J. R.; Scalmani, G.; Barone, V.; Mennucci, B.; Petersson, G. A.; Nakatsuji, H.; Caricato, M.; Li, X.; Hratchian, H. P.; Izmaylov, A. F.; Bloino, J.; Zheng, G.; Sonnenberg, J. L.; Hada, M.; Ehara, M.; Toyota, K.; Fukuda, R.; Hasegawa, J.; Ishida, M.; Nakajima, T.; Honda, Y.; Kitao, O.; Nakai, H.; Vreven, T; A, M. J. J.; Peralta, J. E.; Ogliaro, F.; Bearpark, M.; Heyd, J. J.; Brothers, E.; Kudin, K. N.; Staroverov, V. N.; Kobayashi, R.; Normand, J.; Raghavachari, K.; Rendell, A.; Burant, J. C.; Iyengar, S. S.; Tomasi, J.; Cossi, M.; Rega, N.; Millam, J. M.; Klene, M.; Knox, J. E.; Cross, J. B.; Bakken, V.; Adamo, C.; Jaramillo, J.; Gomperts, R.; Stratmann, R. E.; Yazyev, O.; Austin, A. J.; Cammi, R.; Pomelli, C.; Ochterski, J. W.; Martin, R. L.; Morokuma, K.; Zakrzewski, V. G.; Voth, G. A.; Salvador, P.; Dannenberg, J. J.; Dapprich, S.; Daniels, A. D.; Farkas, ; Foresman, J. B.; Ortiz, J. V.; Cioslowski, J.; Fox, D. J. *Gaussian 09*, Revision A.1; Gaussian, Inc.: Wallingford, CT, 2009.
(99) Herzberg, G. *Molecular Spectra and Molecular Structure: Spectra of Diatomic Molecules*; Van Nostrand Reinhold: New York, 1950.
(100) Neese, F. *J. Chem. Phys.* **2001**, *115*, 11080−11096.
(101) Peterson, K. A.; Dunning, T. H., Jr. *J. Chem. Phys.* **1997**, *106*, 4119−4140.
(102) Rega, N.; Cossi, M.; Barone, V. *J. Chem. Phys.* **1996**, *105*, 11060−11067.
(103) Tanimoto, M.; Saito, S.; Hirota, E. *J. Chem. Phys.* **1986**, *84*, 1210−1214.
(104) Knight, L. B., Jr.; Easley, W. C.; Weltner, W., Jr. *J. Chem. Phys.* **1971**, *54*, 1610−1617.
(105) Knight, L. B., Jr.; Wise, M.; Davidson, E.; McMurchie, L. *J. Chem. Phys.* **1982**, *76*, 126−136.
(106) Knight, L. B., Jr.; Herlong, J. O.; Kirk, T. J.; Arrington, C. *J. Chem. Phys.* **1992**, *96*, 5604−5613.
(107) Piltch, N. D.; Szanto, P. G.; Anderson, T. G.; Gudeman, C. S.; Dixon, T. A.; Woods, R. C. *J. Chem. Phys.* **1982**, *76*, 3385−3388.
(108) Knight, L. B., Jr.; Steadman, J. *J. Chem. Phys.* **1982**, *77*, 1750−1756.
(109) Knight, L. B., Jr.; Steadman, J. *J. Am. Chem. Soc.* **1984**, *106*, 900−902.
(110) Fernandez, B.; Jørgensen, P.; Byberg, J.; Olsen, J.; Helgaker, T.; Jensen, H. J. A. *J. Chem. Phys.* **1992**, *97*, 3412−3419.

(111) Easley, W. C.; Weltner, W., Jr. *J. Chem. Phys.* **1970**, *52*, 197−205.
(112) Knight, L., Jr.; Weltner, W., Jr. *J. Chem. Phys.* **1971**, *55*, 5066−5077.
(113) Yamada, C.; Cohen, E. A.; Fujitake, M.; Hirota, E. *J. Chem. Phys.* **1990**, *92*, 2146−2149.
(114) Kutzelnigg, W.; Fleischer, U.; Schindler, M. *NMR Basic Principles and Progress*; Springer-Verlag: Heidelberg, Germany, 1990.
(115) Ishii, N.; Shimizu, T. *Chem. Phys. Lett.* **1994**, *225*, 462−466.
(116) Chipman, D. M. In *Quantum Mechanical Electronic Structure Calculations with Chemical Accuracy*; Langhoff, S. R., Ed.; Kluwer Academic Publisher: Dordrecht, The Netherlands, 1995; Vol. *13*, pp 109−138.
(117) Perera, S. A.; Salemi, L. M.; Bartlett, R. J. *J. Chem. Phys.* **1997**, *106*, 4061−4066.
(118) Al Derzi, A. R.; Fau, S.; Bartlett, R. J. *J. Phys. Chem. A* **2003**, *107*, 6656−6667.